Electronic Supplementary Material (ESI) for Materials Horizons.
This journal is © The Royal Society of Chemistry 2023

Supporting Information

Order-disorder engineering of RuO_2 nanosheets towards pH-universal oxygen evolution

Yu Zhang, Yuefeng Zhang, Zhiyuan Zeng, and Derek Ho**

Experimental methods

Materials: Ruthenium (III) chloride hydrate (99.9%), cobalt nitrate hexahydrate (98%), ethanol (95%), and 2-methylimidazole (99%) were purchased from Aladdin Group. Nitric acid (69%), sulfuric acid (98%), and perfluorinated resin solution containing Nafion (5 wt%) were purchased from Sigma-Aldrich. Commercial carbon cloth (CC) was purchased from AvCarb.

Synthesis of Co-MOF/CC: Carbon cloth (CC) was first functionalized by the mixture of nitrate acid and sulfide acid with V_{HNO3}/V_{H2SO4}=3:1 for more than 24 h. Then, it was rinsed by DI water several times and dried at 60 ^{o}C. A piece of 3 cm*3 cm functionalized CC was vertically immersed in the 40 mL mixed solution containing 0.657 g of 2-methylimidazole and 0.291 g of cobalt nitrate hexahydrate. After keeping the CC in the solution for 6 h at room temperature, the Co-MOF supported on CC, denoted as Co-MOF/CC, was obtained by washing with DI water and drying at 60 ^{o}C overnight.

Synthesis of a/c-RuO_2/CC: A piece of Co-MOF/CC was immersed in 20 mL ruthenium chloride hydrate aqueous solution with a concentration of 2 mg mL^{-1} for 3 h at room temperature, which was subsequently rinsed by DI water and dried at 60 ^{o}C overnight to obtain $Ru(OH)_x$/CC. Subsequently, the a/c-RuO_2/CC was obtained via thermal treatment with $Ru(OH)_x$/CC in the muffle furnace at 250 ^{o}C for 2 h, with a heating rate of 5 ^{o}C min^{-1} in air. The mass loading of RuO_2 on carbon cloth was calculated to be 1.0 mg cm^{-2}. For comparison, a-RuO_2/CC and c-RuO_2/CC samples with the same loading density of about 1.0 mg cm^{-2} were prepared via thermal treatment with $Ru(OH)_x$/CC at 150 ^{o}C and 350 ^{o}C for 2 h, respectively.

Preparation of commercial RuO_2/CC: 10 mg commercial RuO_2 was dispersed in 2 mL mixed solution containing 1600 μL of DI water, 350 μL of absolute ethanol, and 50 μL Nafion before ultrasonicating for 30 min to form a homogenous ink. 100 μL ink was then dropped on both sides of the CC (0.5 * 0.5 cm) to prepare the commercial RuO_2/CC with a mass loading of 1.0 mg cm^{-2}.

Electrochemical measurements

The electrochemical OER tests were carried out in 1 M KOH, 1 M PBS, and 0.5 M H_2SO_4, respectively, with a standard three-electrode system in an electrochemical workstation (Chenhua, CHI 660E). $HgSO_4$/Hg, $HgCl_2$/Hg, and HgO/Hg electrodes were utilized as reference electrodes in acidic, neutral, and alkaline electrolyte,

respectively. Graphite rod was used as counter electrode. All the electrolytes used in electrolyte measurements were saturated with O_2. All potentials were converted to the reversible hydrogen electrode (RHE) scale. The geometric size of the working electrode is set as 0.5 cm * 0.5 cm. The linear sweep voltammograms (LSV) curves were collected at a scan rate of 5 mV s^{-1}, and were 100 % corrected for IR loss (IR corrected polarization curves makes up for the electrode potential loss at medium to high current region caused by the solution resistance (R_S)). The compensated potential ($E_{compensated}$) was recorded using the following formula: $E_{compensated} = E_{measured} - i \times R_S$, where R_S was determined by the electrochemical workstation. The electrochemical impendence spectroscopy (EIS) measurements under acidic, alkaline, and neutral conditions were measured at potentials of 1.60, 1.60, and 1.65 V, respectively, in the frequency range of 0.1 to 100k Hz with an amplitude of 5 mV. The durability of all the as-prepared catalysts in 0.5 M H_2SO_4 was evaluated by using chronopotentiometric tests at a constant current density of 10 mA cm^{-2}, and the stability of a/c-RuO_2/CC was further measured in 0.5 M H_2SO_4 using chronopotentiometric tests at 50 mA cm^{-2}. The stability tests of a/c-RuO_2/CC in acidic, alkaline, and neutral electrolytes were also carried out by cyclic voltammetry (CV) sweeps from 1.2 to 1.4 V, 1.2 to 1.5 V, and 1.2 to 1.6 V, respectively, at the scan rate of 50 mV s^{-1} for 2000 cycles. The electrochemical active surface area (ECSA) was calculated from the CV curves using the following equation: $C_{dl} = (j_a - j_c)/(2 \bullet \nu) = \Delta j/(2 \bullet \nu)$, where C_{dl}, j_a, j_c and ν are the double-layer capacitance (F cm^{-2}), the anodic current density (mA cm^{-2}), the cathodic current density (mA cm^{-2}), and scan rate (mV s^{-1}), respectively. ECSA = $C_{dl}/C_{dl,ideal}$, where $C_{dl,ideal}$ is the specific capacitance of an ideally flat electrode. It is usually taken as 35 and 40 μF cm^{-2} for acidic and alkaline (neutral) solutions, respectively.[1]

Materials characterizations

Scanning electron microscopy (SEM) was carried out on a field emission scanning electron microscope (JEOL, JSM-6335F) with a scan voltage of 5 KV. Transmission electron microscopy (TEM) operated at 200 kV was recorded on by a high-resolution TEM (HRTEM, JEOL, 2100F). X-ray diffraction (XRD) patterns (2θ, 10-90°) were collected on a Bruker D2 Phaser X-ray diffractometer. The lattice strain measurement at the amorphous-crystalline boundary was carried out using the geometric phase analysis of the HRTEM image,[2] where e_{yy} and e_{xx} components of the strain tensor in a/c-RuO_2/CC can be obtained. X-ray photoelectron spectroscopy (XPS) was acquired by a Physical Electronic PHI 5f02 X-ray photoelectron spectrometer incorporating an

11-inch spherical capacitor analyzer and a monochromatic Al Kα (1486.6 eV) radiation at 350 W (15 kV, 23 mA). The binding energies were determined using the C1s line at 284.6 eV with adventitious carbon as a reference. Ultraviolet photoelectron spectroscopy (UPS) was performed on Thermo Scientific™ K-Alpha using He I resonance lines (hν = 21.22 eV), and the work function (Φ) is calculated by using the following equation: $\Phi = h\nu + E_{cutoff} - E_F$ (E_{cutoff} refers to the secondary electron cutoff energy and is obtained from the intersection of tangential lines drawn on the high-binding-energy cutoff of the UPS spectrum with the zero intensity line, while E_F refers to the Fermi level and is taken as 0).[3, 4] Raman spectra were carried out on a confocal Raman spectrometer (WITec alpha300 R) with an excitation wavelength of 532 nm and a laser power of 3 mW. The oxygen vacancy defects were identified by electron spin resonance (ESR, Magnettech MS-5000X). Inductively coupled plasma optical emission spectrometry (ICP-OES) measurements were carried on Agilent 720ES.

Calculation method:

All DFT calculations were carried out through the Vienna *ab-initio* Simulation Package (VASP).[5] The exchange-correlation interactions were described by the generalized gradient approximation (GGA)[6] within the framework of the Perdew−Burke−Ernzerhof functional (PBE).[7] The energy cutoff for the planewave basis set was set to 520 eV for all the calculations. The van der Waals interaction were treated by employing the empirical corrections by Grimme et al. (DFT-D3).[8] The optimized bulk RuO_2 lattice parameters (a = 4.53 Å, b = 4.53 Å and c = 3.13 Å) are consistent with the experimental lattice parameters value. To simulate the amorphous structures, the expanded supercell model was relaxed at 1400 K over a total period of 15 ps with a time step of 3 fs with the ab inito molecular dynamics method. According to the experimental results, we cleave (110) faces from the bulk structure to study the OER activity. The k-point sampling of the Brillioun zone adopted a 2 × 2 × 1 grid centered at the gamma point to optimize the pristine (110) surface and amorphous (110) surface containing 32 Ru atoms and 64 O atoms, respectively, and a 1 × 1 × 1 k-points grid to optimize the heterostructure including 192 atoms. For pristine (110) surface, we fixed the bottom two atomic layers, and the other atomic layers and the adsorbates were allowed to move freely until reaching the convergence criteria. While for amorphous and heterostructures, we relax the top two atomic layers, and the other layers are fixed. Spin-polarization were considered in all the calculations. Geometry optimizations were carried out until the residual force and energy acting on the atoms were below 0.02

eV/Å and 10^{-6} eV, respectively. The vacuum thickness was set to 16 Å to avoid the interaction between the slab and its periodical images.

The Gibbs free energy change (ΔG) was calculated as

$$\Delta G = \Delta E_{DFT} + \Delta E_{ZPE} - T\Delta S - eU$$

where ΔE_{DFT} is the reaction energy obtained from the DFT calculations, ΔE_{ZPE} is the zero-point energy, S is the standard entropy obtained from NIST database and T is room temperature (298.15 K). U is the potential against standard hydrogen electrode (SHE) and e is the transferred charge.

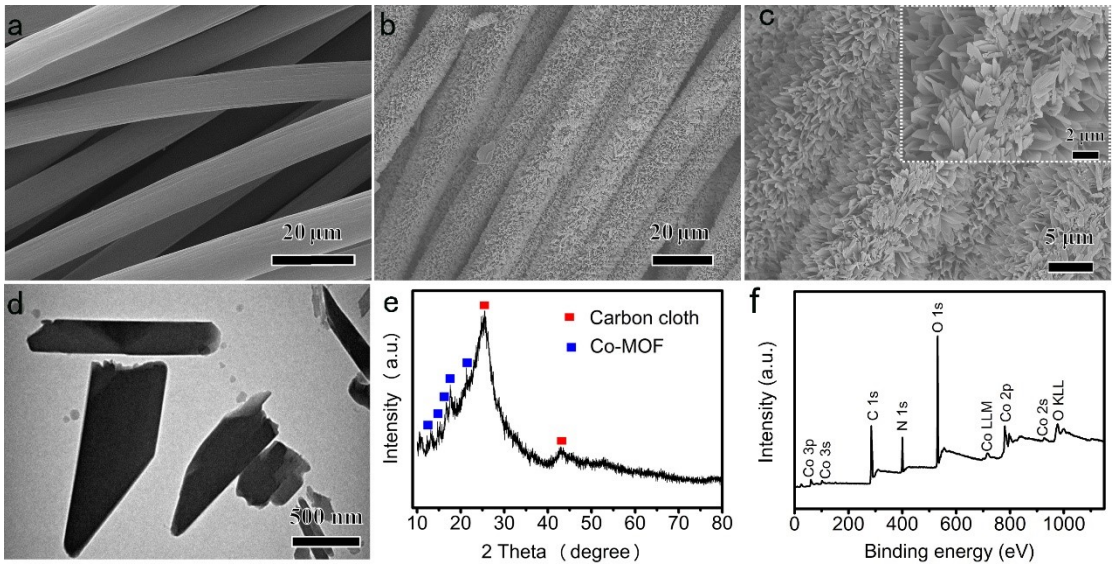

Fig. S1. (a) SEM image of pristine CC. (b-c) SEM images (the inset is the enlarged image), (d) TEM image, (e) XRD pattern, and (f) XPS survey spectrum of Co-MOF/CC.

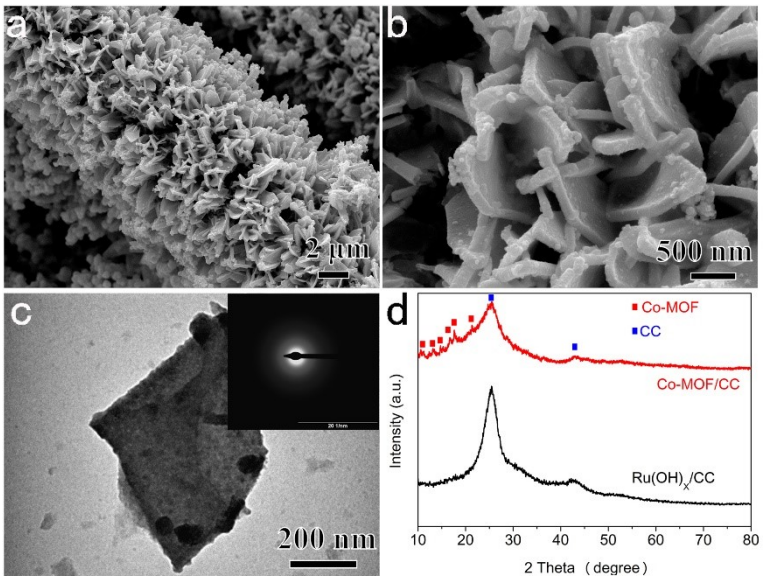

Fig. S2. (a,b) SEM images and (c) TEM image of $Ru(OH)_x$/CC (the inset is the corresponding SAED pattern). (d) XRD patterns of Co-MOF/CC and $Ru(OH)_x$/CC.

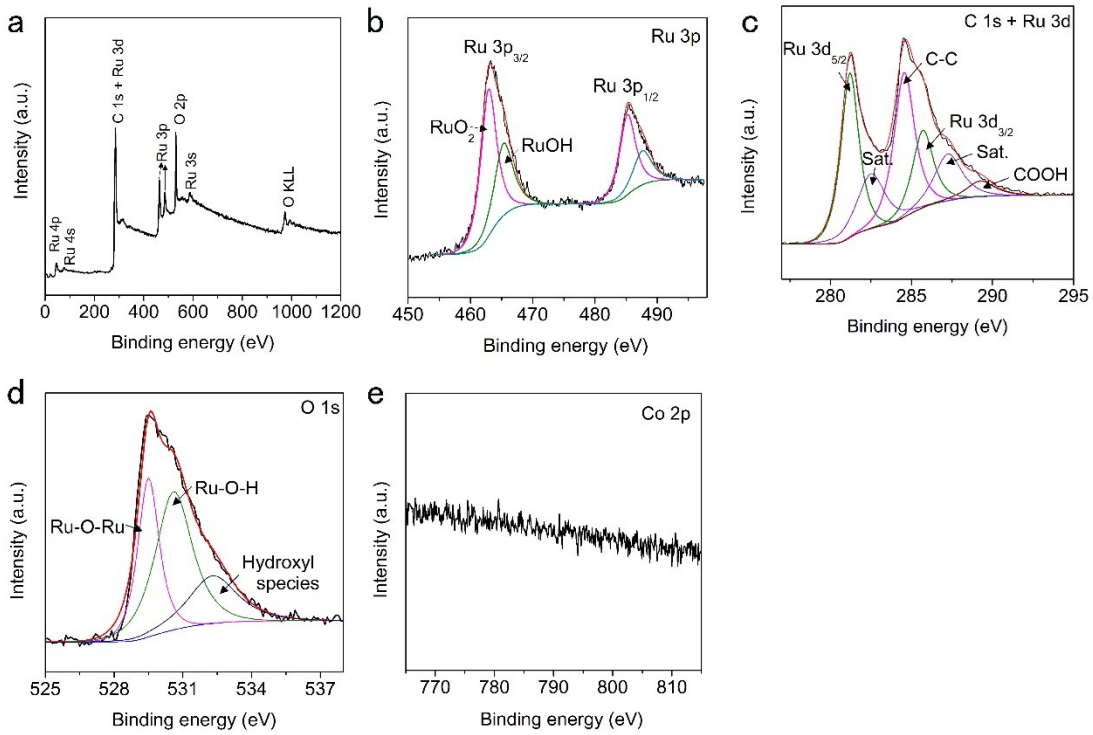

Fig. S3. (a) XPS survey spectrum of $Ru(OH)_X$/CC. (b-e) XPS spectra of Ru 3p (b), Ru 3d+C 1s (c), O 1s (d), and Co 2p (e) in $Ru(OH)_X$/CC.

The chemical states of the as-prepared $Ru(OH)_X$/CC were investigated using XPS analysis. The XPS survey spectrum (Fig. S3a) confirms the co-existence of Ru and O elements. The Ru $3p_{3/2}$ spectrum (Fig. S3b) is deconvoluted into two peaks located at 463.0 and 465.5 eV, corresponding to RuO_2 and RuOH, respectively.[9] The C 1s XPS spectrum (Fig. S3c) seems to be relatively complex owing to the overlap with Ru 3d region. The C 1s peak at 284.6 eV, from adventitious carbon and our CC substrate, is utilized for binding energy calibration. The peak at 289.2 eV is assigned to -COOH species from the CC substrate that was functionalized by the mixture of nitric acid and sulfuric acid prior to use.[10] The remaining peaks in Fig. S3c belong to the Ru 3d peaks and their corresponding satellite peaks. The O 1s spectrum (Fig. S3d) is deconvoluted into three components: Ru-O-Ru (529.4 eV), Ru-O-H (530.7 eV), and surface hydroxyl species (532.4 eV). The absence of Co 2p signal (Fig. S3e) suggests the complete removal of Co-MOF template during the conversion from Co-MOF/CC to $Ru(OH)_X$/CC.

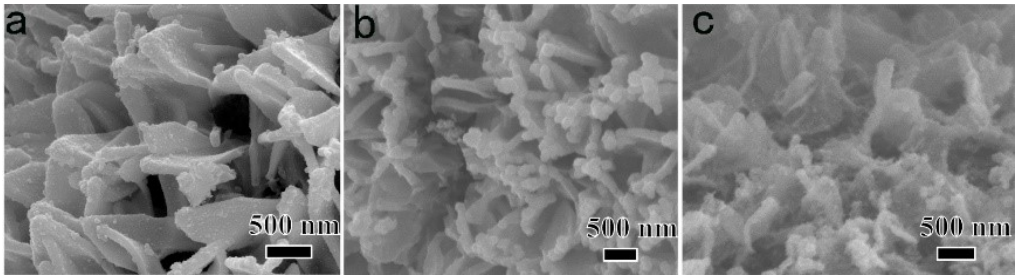

Fig. S4. SEM images of a-RuO_2/CC (a), a/c-RuO_2/CC (b), and c-RuO_2/CC (c).

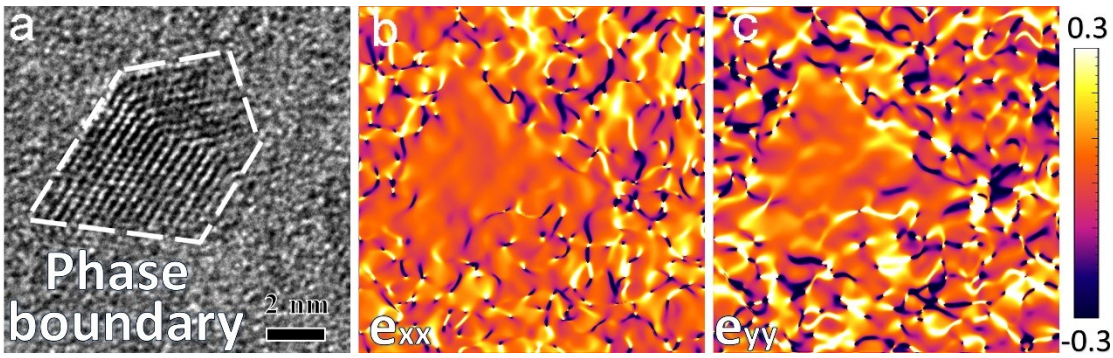

Fig. S5. (a) HRTEM image of a/c-RuO_2/CC, and the corresponding e_{xx} (b) and e_{yy} (c) strain component within the crystalline region performed by geometric phase analysis (GPA).

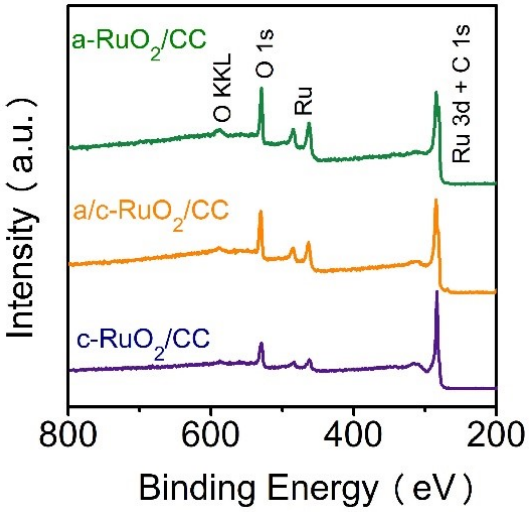

Fig. S6. XPS survey spectra of a-RuO_2/CC, a/c-RuO_2/CC, and c-RuO_2/CC.

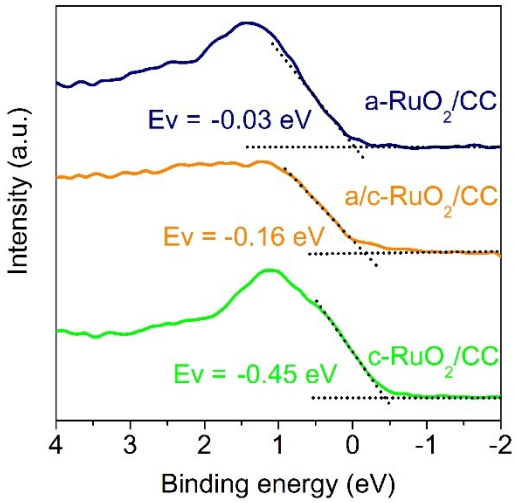

Fig. S7. Valence band (VB) XPS spectra of a-RuO_2/CC, c-RuO_2/CC, and a/c-RuO_2/CC.

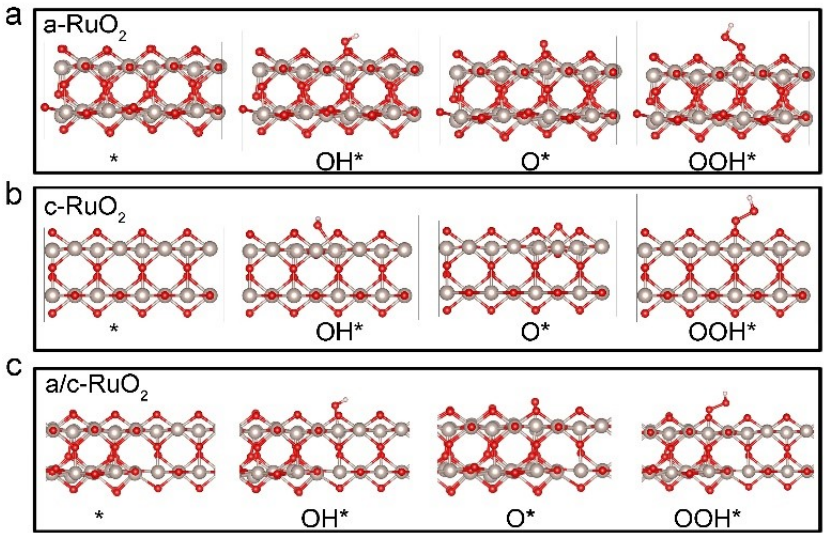

Fig. S8. Calculated reaction pathway for OER over a-RuO_2/CC, c-RuO_2/CC, and a/c-RuO_2/CC.

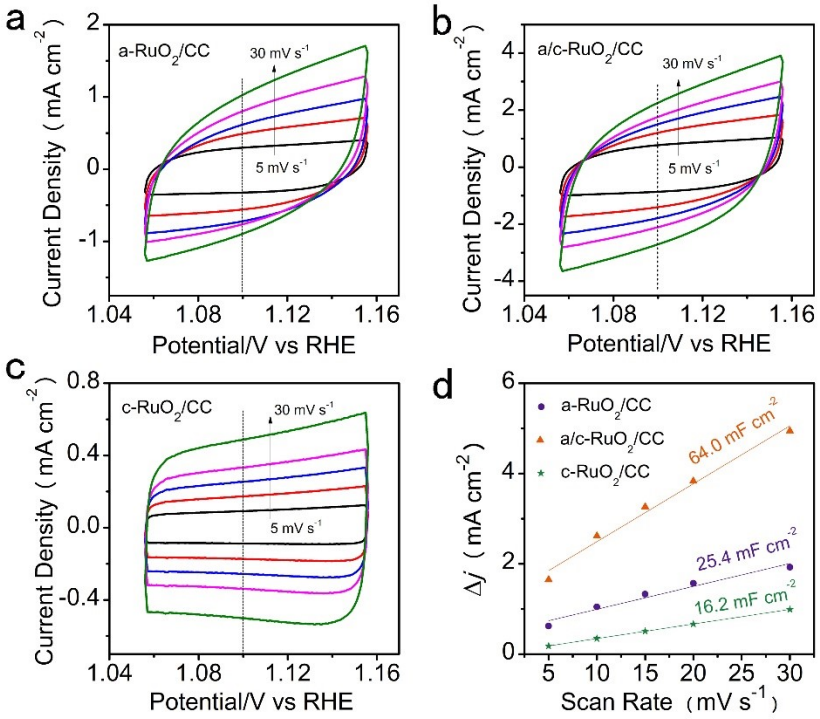

Fig. S9. CV profiles for acidic OER of (a) a-RuO_2/CC, (b) a/c-RuO_2/CC, and (c) c-RuO_2/CC in a non-Faradaic region at the different scan rate range from 5 mV s^{-1} to 30 mV s^{-1}. (d) Plots of Δj ($\Delta j = j_a - j_c$, j_a *and* j_c are recorded at 1.10 V vs RHE) as a function of the scan rate.

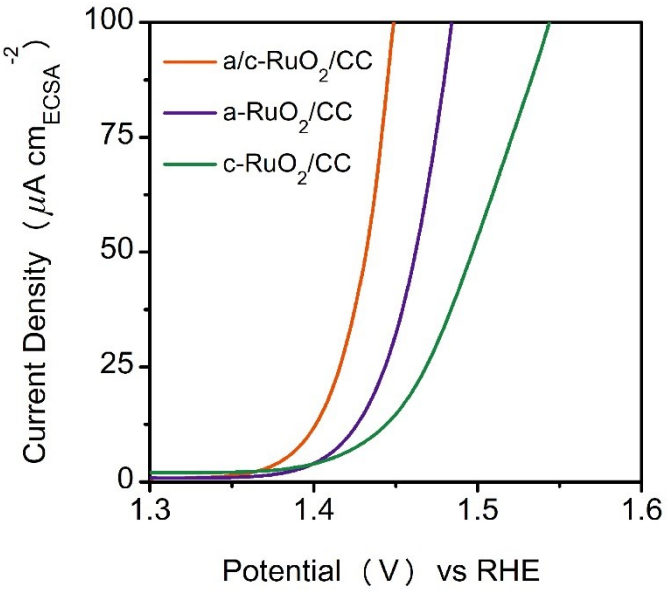

Fig. S10. Specific activity of a-RuO_2/CC, a/c-RuO_2/CC, and c-RuO_2/CC for acidic OER normalized by their corresponding ECSA values (see Table S5).

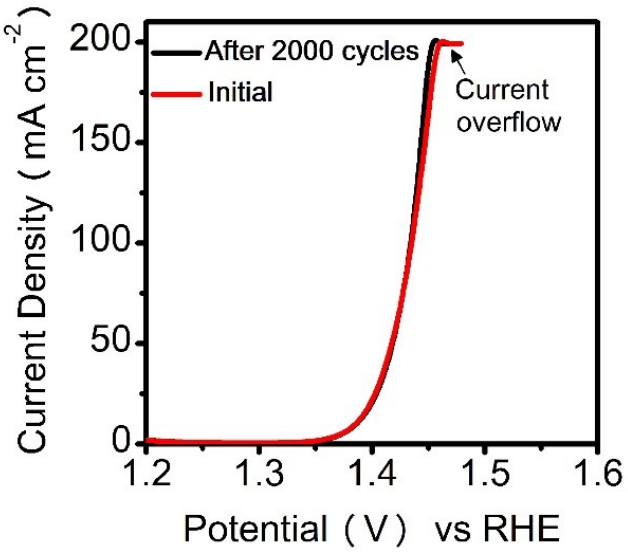

Fig. S11. Polarization curves of a/c-RuO_2/CC before and after 2000 CV cycles in 0.5 M H_2SO_4, and the current overflow observed on the polarization curves is caused by the limitation of the current sensitivity (0.1 A).

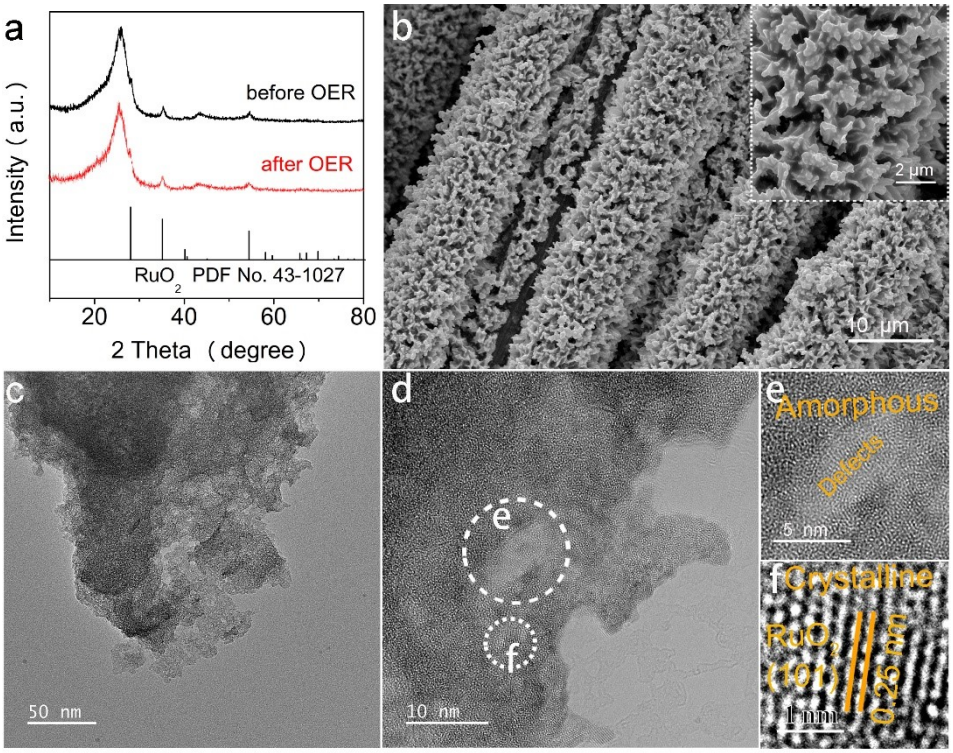

Fig. S12. (a) XRD pattern, (b) SEM image, (c) TEM image, and (d) HRTEM image of the a/c-RuO_2/CC recovered from 24 h chronopotentiometry measurement in 0.5 M H_2SO_4 at 10 mA cm^{-2}. (e-f) The enlarged HRTEM image for the marked area in panel d.

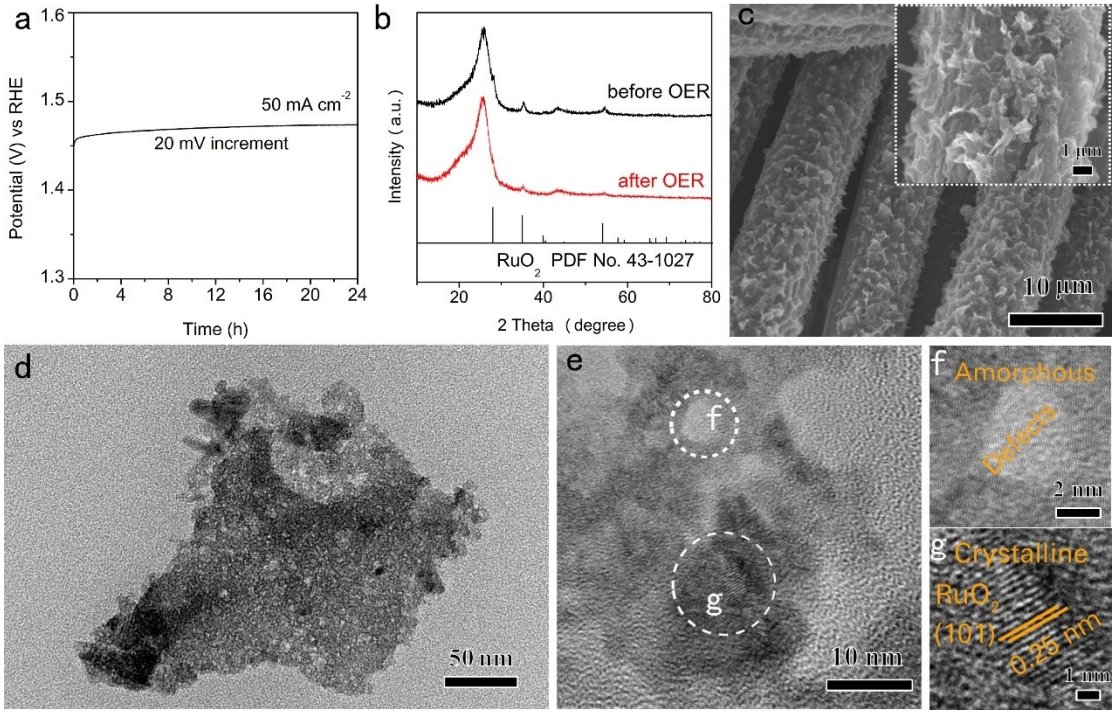

Fig. S13. (a) Chronopotentiometry measurement of a/c-RuO_2/CC in 0.5 M H_2SO_4 at the constant current density of 50 mA cm^{-2}. (b) XRD pattern, (c) SEM image, (d) TEM image, and (e) HRTEM image of the a/c-RuO_2/CC recovered from 24 h chronopotentiometry measurement in 0.5 M H_2SO_4 at 50 mA cm^{-2}. (f-g) The enlarged HRTEM image for the marked area in panel e.

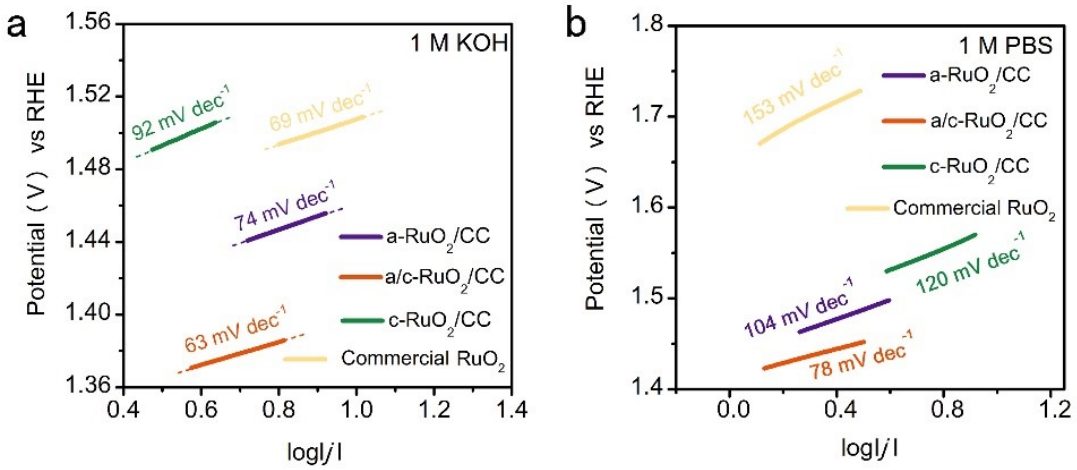

Fig. S14. Tafel slopes of a-RuO_2/CC, a/c-RuO_2/CC, c-RuO_2/CC, and commercial RuO_2 in alkaline (a) and neutral (b) electrolytes.

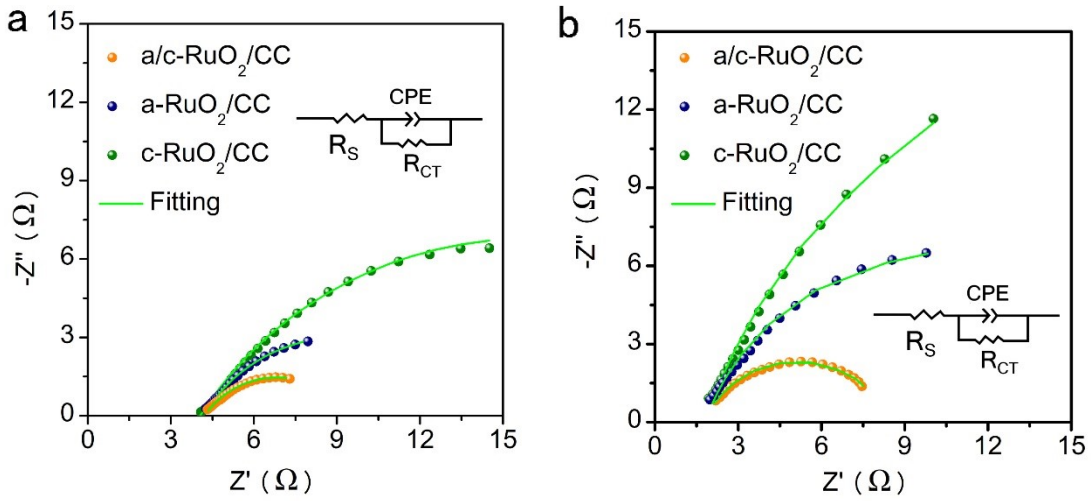

Fig. S15. EIS plots of a-RuO_2/CC, a/c-RuO_2/CC, and c-RuO_2/CC in alkaline (a) and neutral (b) electrolytes measured at 1.60 and 1.65 V vs RHE, respectively, and the inset is the equivalent circuit model.

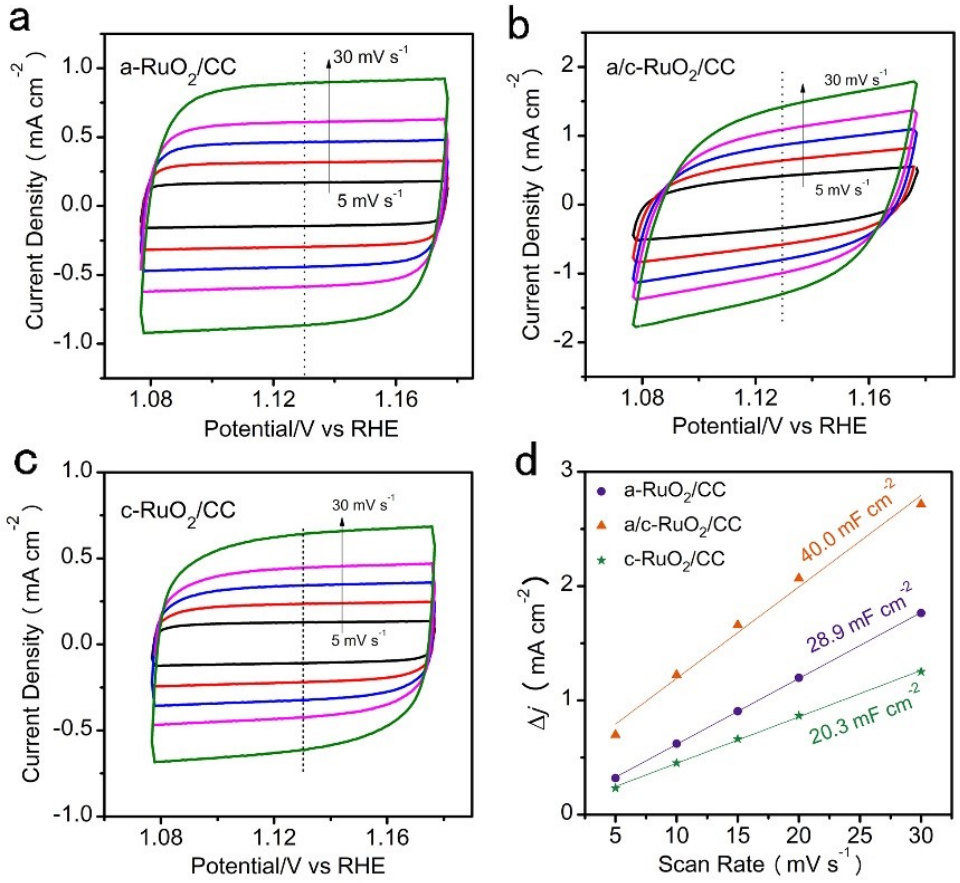

Fig. S16. CV profiles for alkaline OER of (a) a-RuO_2/CC, (b) a/c-RuO_2/CC, and (c) c-RuO_2/CC in a non-Faradaic region at the different scan rate range from 5 mV s^{-1} to 30 mV s^{-1}. (d) Plots of Δj ($\Delta j = j_a - j_c, j_a$ *and* j_c are recorded at 1.13 V vs RHE) as a function of the scan rate.

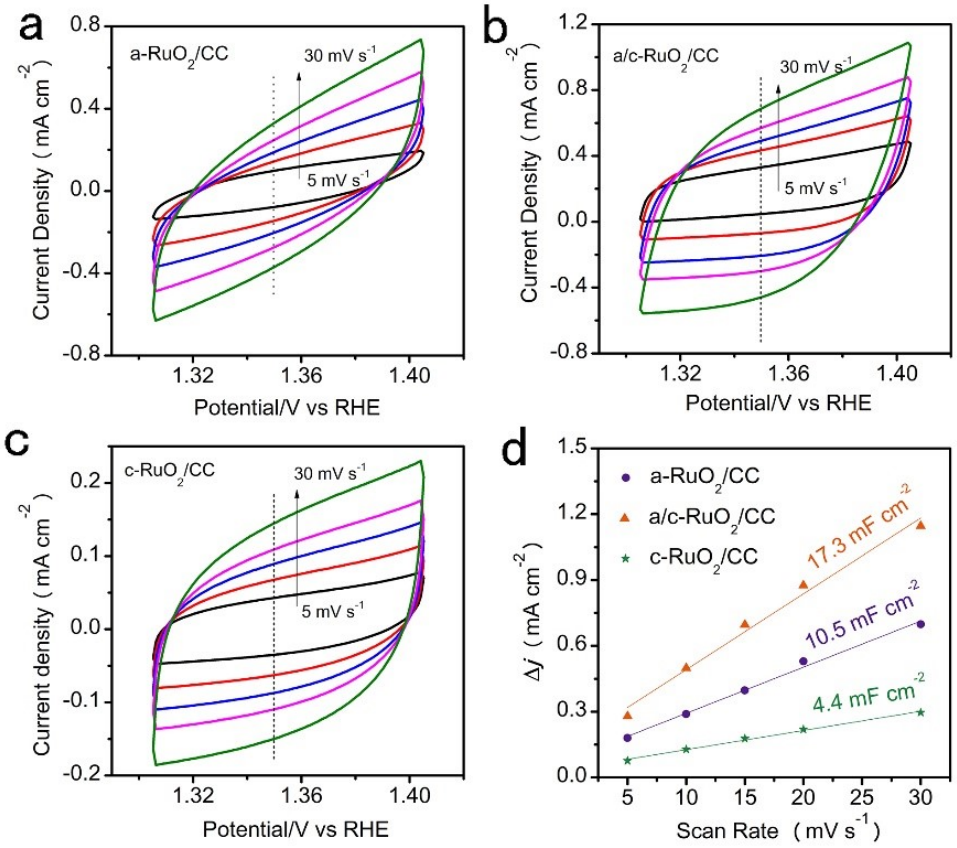

Fig. S17. CV profiles for neutral OER of (a) a-RuO_2/CC, (b) a/c-RuO_2/CC, and (c) c-RuO_2/CC in a non-Faradaic region at the different scan rate range from 5 mV s^{-1} to 30 mV s^{-1}. (d) Plots of Δj ($\Delta j = j_a - j_c$, j_a *and* j_c are recorded at 1.35 V vs RHE) as a function of the scan rate.

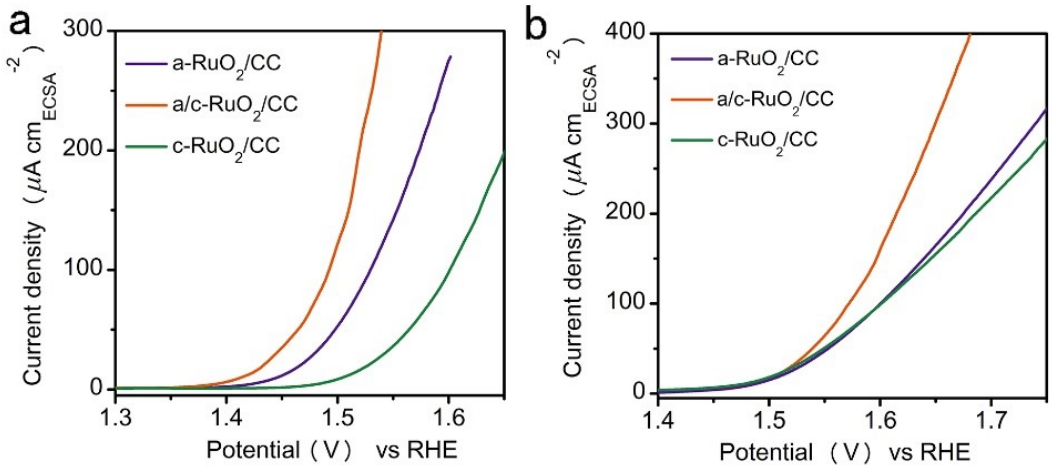

Fig. S18. Specific activities of a-RuO_2/CC, a/c-RuO_2/CC, and c-RuO_2/CC normalized by their corresponding ECSA values under (a) alkaline and (b) neutral conditions.

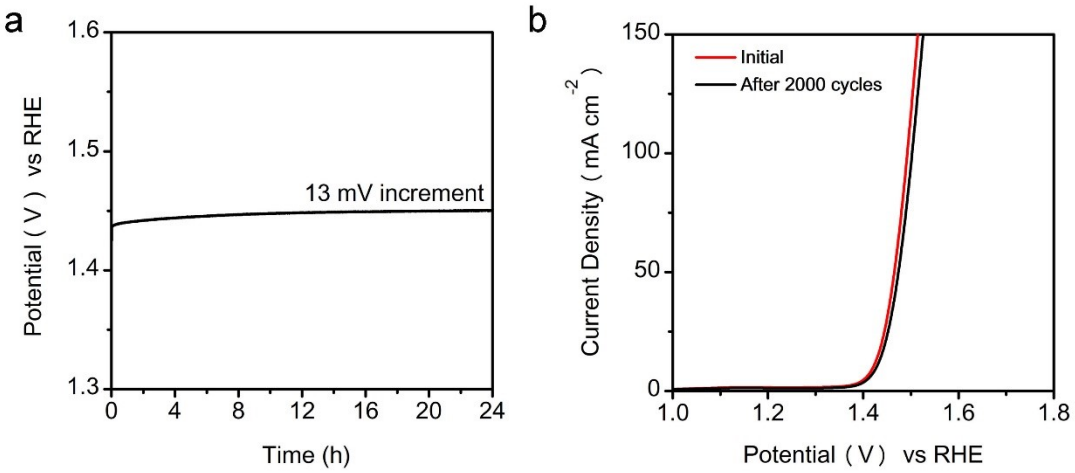

Fig. S19. (a) Chronopotentiometry measurement of a/c-RuO_2/CC in 1 M KOH at the constant current density of 10 mA cm^{-2}. (b) Polarization curves of a/c-RuO_2/CC before and after 2000 CV cycles in the alkaline electrolyte (1 M KOH).

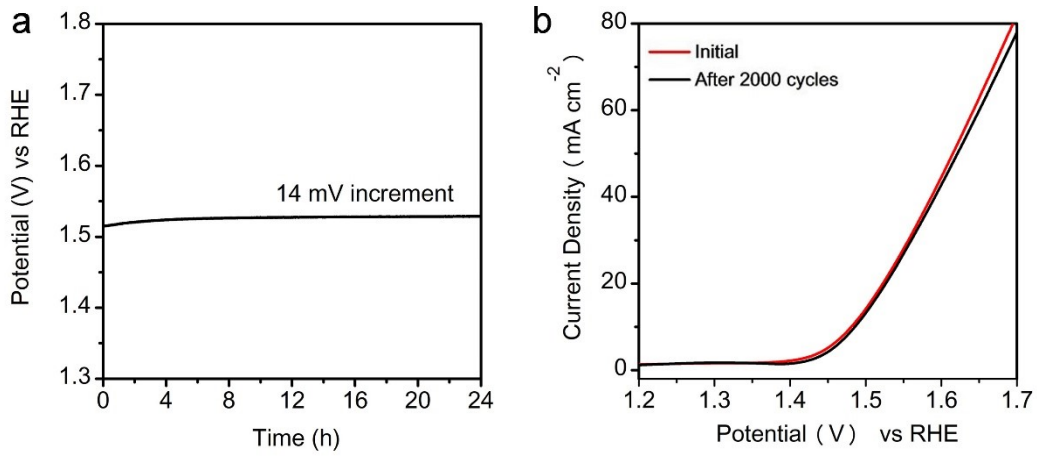

Fig. S20. (a) Chronopotentiometry measurement of a/c-RuO_2/CC in 1 M PBS at the constant current density of 10 mA cm^{-2}. (b) Polarization curves of a/c-RuO_2/CC before and after 2000 CV cycles in the neutral electrolyte (1 M PBS).

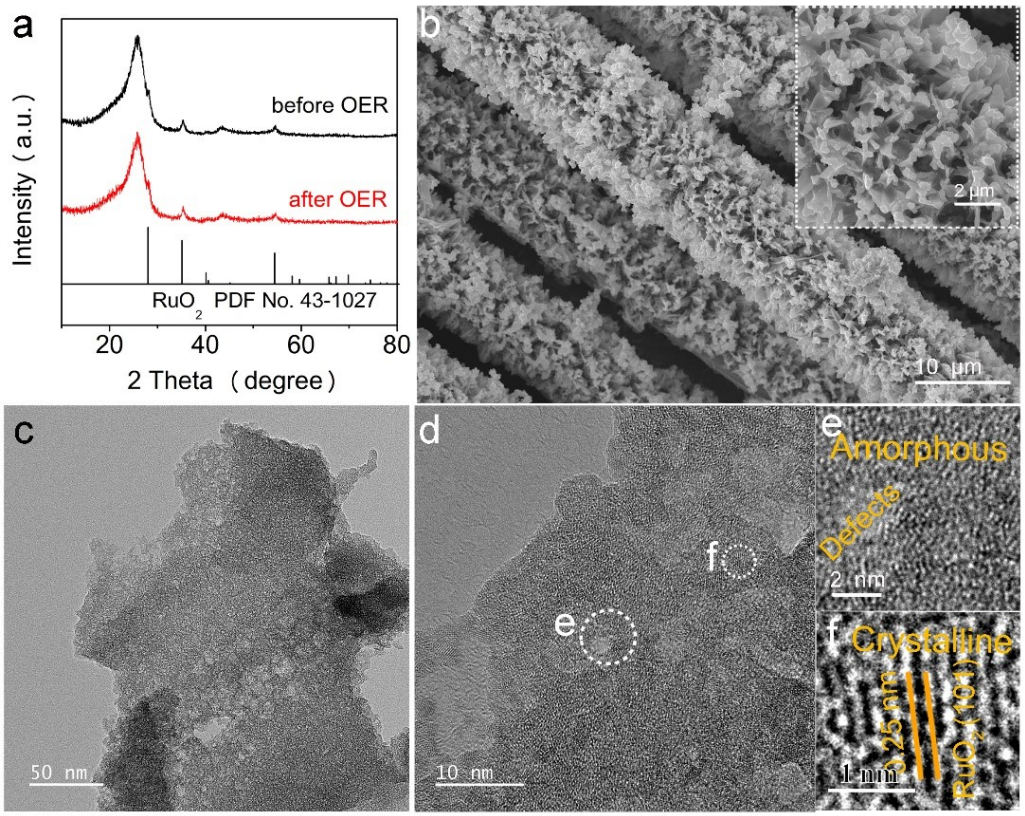

Fig. S21. (a) XRD pattern, (b) SEM image, (c) TEM image, and (d) HRTEM image of the a/c-RuO_2/CC recovered from 24 h chronopotentiometry measurement in 1 M KOH at 10 mA cm^{-2}. (e-f) Enlarged HRTEM image for the marked area in panel d.

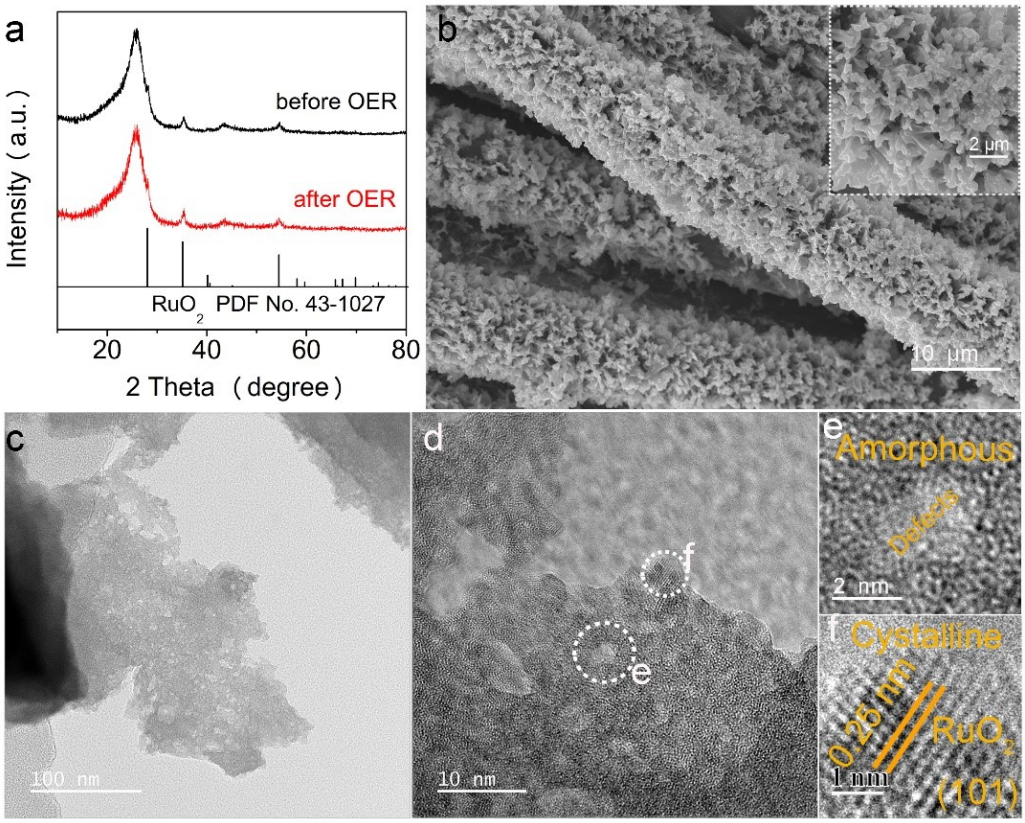

Fig. S22. (a) XRD pattern, (b) SEM image, (c) TEM image, and (d) HRTEM image of the a/c-RuO_2/CC recovered from 24 h chronopotentiometry measurement in 1 M PBS at 10 mA cm^{-2}. (e-f) Enlarged HRTEM image for the marked area in panel d.

Table S1. Fitted results of the EIS plots.

Catalysts	a/c-RuO_2/CC	c-RuO_2/CC	a-RuO_2/CC
R_{CT} (acidic medium)	3.7 Ω	43.0 Ω	10.3 Ω
R_{CT} (alkaline medium)	5.3 Ω	29.1 Ω	10.1 Ω
R_{CT} (neutral medium)	6.5 Ω	38.0 Ω	17.4 Ω

Table S2. The calculated E_{cutoff}, work function (Φ), and E_v values of c-RuO_2/CC, a/c-RuO_2/CC, and a-RuO_2/CC.

Catalysts	c-RuO_2/CC	a/c-RuO_2/CC	a-RuO_2/CC
E_{cutoff}	15.37 eV	14.93 eV	14.65 eV
Φ	5.85 eV	6.29 eV	6.57 eV
E_v	-0.45 eV	-0.16 eV	-0.03 eV

Table S3. The OER activity comparison of a/c-RuO_2/CC, a-RuO_2/CC, and c-RuO_2/CC under alkaline and neutral conditions. Note that *n.a.* means not available.

Electrolyte	Overpotential (η)	a/c-RuO_2/CC	a-RuO_2/CC	c-RuO_2/CC	Commercial RuO_2
0.5 M H_2SO_4	η_{10}	150 mV	198 mV	234 mV	390 mV
	η_{100}	203 mV	267 mV	405 mV	*n.a.*
1 M KOH	η_{10}	184 mV	225 mV	297 mV	271 mV
	η_{100}	263 mV	319 mV	421 mV	356 mV
1 M PBS	η_{10}	261 mV	317 mV	370 mV	532 mV

Table S4. OER catalytic performance comparison of the proposed a/c-RuO_2/CC sample with respect to recently reported Ru-based catalysts in acidic environment. Note that *n.a.* means not available.

Material	η (mV) @10/100 mA cm^{-2}	Tafel slope (mV dec^{-1})	Ref.
a/c-RuO_2/CC	150/203	48	This work
$Li_{0.52}RuO_2$	157/250	83	[11]
Mn-RuO_2	158/255	43	[12]
Ru_3MoCeO_x	164/230	61	[13]
2D D-RuO_2/G	169/220	40	[14]

UfD-RuO_2/CC	179/ *n.a.*	37	[15]
RuO_2/D-TiO_2	180/239	43	[10]
Ru/Se-RuO_2	190/240	44	[16]
E–Zn–RuO_2	190/220	51	[17]
$Ru_1Ir_1O_x$	204/290	71	[18]
PtCo–RuO_2/C	212.6 ± 5.3/*n.a.*	49	[19]
SS Pt-RuO_2 HNSs	228/ *n.a.*	51	[20]
Ru5W1Ox	234/ *n.a.*	42	[21]
E-Ru/Fe ONAs	238/ *n.a.*.	45	[22]

Table S5. The calculated ECSA values of different samples by using the following equation: ECSA=$C_{dl}/C_{dl,ideal}$. The $C_{dl,ideal}$ values for acidic and alkaline (neutral) solutions are taken as 35 and 40 μF cm^{-2}, respectively.

	a/c-RuO_2/CC	a-RuO_2/CC	c-RuO_2/CC
ECSA (acid condition)	1828.6	725.7	462.8
ECSA (neutral condition)	432.5	262.5	110
ECSA (alkaline condition)	1000	722.5	507.5

Table S6. OER catalytic performance comparison of the proposed a/c-RuO_2/CC sample with respect to recently reported Ru-based catalysts under alkaline conditions. Note that *n.a*. means not available.

Material	η (mV) @10/100 mA cm^{-2}	Tafel slope (mV dec^{-1})	Ref.
a/c-RuO_2/CC	184/263	63	This work
RuO_2@Co_3O_4	152/198	68	[23]
RuO_2/CoO_x	165/230	*n.a*.	[24]
Mn-RuO_2	175/260	16	[14]
RuO_2/NiFeOOH	188/250	32	[25]
Ru/RuO_2	189/*n.a*.	68	[26]
Co-SAC/RuO_2	200/*n.a*.	110	[27]
Ru−RuO_2	223/300	79	[28]
NiFeRu-LDH	225/255	*n.a*.	[29]
RuCu NSs	234/*n.a*.	15	[30]
$RuIrO_x$	250/*n.a*.	50	[31]
CoNiRu-NT	255/330	67	[32]
$RuTe_2$-PNRs	285/*n.a*.	62	[33]

Table S7. OER catalytic performance comparison of the proposed a/c-RuO_2/CC sample with respect to recently reported Ru-based catalysts under neutral conditions. Note that *n.a*. means not available.

Material	η (mV) @10 mA cm^{-2}	Tafel slope (mV dec^{-1})	Ref.
a/c-RuO_2/CC	261	78	This work
RuO_2/CoO_x	242	70	[24]
$RuIrCaO_x$	250	*n.a*.	[34]
0.27-RuO_2@C	269	116	[35]
Ru-RuO_2/CNT	275	97	[36]
7Å-RuO_2	290	*n.a*.	[37]
B-RuO_2	290	*n.a*.	[38]
IrRu@Te	309	*n.a*.	[39]
Ru-RuO_2/C_3N_4	342	92	[40]
RuO_2/Co_3O_4	365	53	[41]
Ru-RuO_2@NPC	440	*n.a*.	[42]

Reference

1. C. C. McCrory, S. Jung, J. C. Peters and T. F. Jaramillo, *J. Am. Chem. Soc.*, 2013, **135**, 16977-16987.
2. M. Hÿtch, *Scanning Microsc*, 1997, **11**, 53-66.
3. T. Liu, C. Xi, C. Dong, C. Cheng, J. Qin, S. Hu, H. Liu and X.-W. Du, *J. Phy. Chem.C*, 2019, **123**, 28319-28326.
4. C. Wang, H. Lu, Z. Mao, C. Yan, G. Shen and X. Wang, *Adv. Funct. Mater.*, 2020, **30**, 2000556.
5. S. Anantharaj, S. Ede, K. Karthick, S. S. Sankar, K. Sangeetha, P. Karthik and S. Kundu, *Energy Environ. Sci.*, 2018, **11**, 744-771.
6. J. P. Perdew, K. Burke and M. Ernzerhof, *Phy. Rev. Lett.*, 1996, **77**, 3865.
7. J. P. Perdew, M. Ernzerhof and K. Burke, *J. Chem. Phy.*, 1996, **105**, 9982-9985.
8. S. Grimme, *J. Comput. Chem.*, 2006, **27**, 1787-1799.
9. W. Wang, S. Guo, I. Lee, K. Ahmed, J. Zhong, Z. Favors, F. Zaera, M. Ozkan and C. S. Ozkan, *Sci. Rep.*, 2014, **4**, 4452.
10. X. Wang, X. Wan, X. Qin, C. Chen, X. Qian, Y. Guo, Q. Xu, W.-B. Cai, H. Yang and K. Jiang, *ACS Catal.*, 2022, **12**, 9437-9445.

11. Y. Qin, T. Yu, S. Deng, X.-Y. Zhou, D. Lin, Q. Zhang, Z. Jin, D. Zhang, Y.-B. He and H.-J. Qiu, *Nat. Commun.*, 2022, **13**, 3784.
12. S. Chen, H. Huang, P. Jiang, K. Yang, J. Diao, S. Gong, S. Liu, M. Huang, H. Wang and Q. Chen, *ACS Catal.*, 2019, **10**, 1152-1160.
13. J. He, W. Li, P. Xu and J. Sun, *Appl. Catal. B*, 2021, **298**, 120528.
14. Y. Li, Y. Wang, J. Lu, B. Yang, X. San and Z.-S. Wu, *Nano Energy*, 2020, **78**, 105185.
15. R. Ge, L. Li, J. Su, Y. Lin, Z. Tian and L. Chen, *Adv. Energy Mater.*, 2019, **9**, 1901313.
16. K. Huang, C. Lin, G. Yu, P. Du, X. Xie, X. He, Z. Zheng, N. Sun, H. Tang and X. Li, *Adv. Funct. Mater.*, 2022, 2211102.
17. Y.-N. Zhou, N. Yu, Q.-X. Lv, B. Liu, B. Dong and Y.-M. Chai, *J. Mater. Chem. A*, 2022, **10**, 16193-16203.
18. J. He, X. Zhou, P. Xu and J. Sun, *Adv. Energy Mater.*, 2021, **11**, 2102883.
19. H. Jin, S. Choi, G. J. Bang, T. Kwon, H. S. Kim, S. J. Lee, Y. Hong, D. W. Lee, H. S. Park and H. Baik, *Energy Environ. Sci.*, 2022, **15**, 1119-1130.
20. J. Wang, H. Yang, F. Li, L. Li, J. Wu, S. Liu, T. Cheng, Y. Xu, Q. Shao and X. Huang, *Sci. Adv.*, 2022, **8**, eabl9271.
21. Y. Wen, C. Liu, R. Huang, H. Zhang, X. Li, F. P. García de Arquer, Z. Liu, Y. Li and B. Zhang, *Nat. Commun.*, 2022, **13**, 4871.
22. Q. Yao, B. Huang, Y. Xu, L. Li, Q. Shao and X. Huang, *Nano Energy*, 2021, **84**, 105909.
23. Y. Jiang, H. Liu, Y. Jiang, Y. Mao, W. Shen, M. Li and R. He, *Appl. Catal. B*, 2023, **324**, 122294.
24. K. Du, L. Zhang, J. Shan, J. Guo, J. Mao, C.-C. Yang, C.-H. Wang, Z. Hu and T. Ling, *Nat. Commun.*, 2022, **13**, 5448.
25. G. Chang, Y. Zhou, J. Wang, H. Zhang, P. Yan, H. B. Wu and X. Y. Yu, *Small*, 2023, **19**, 2206768.
26. S. L. Nicole, Y. Li, W. Xie, G. Wang and J. M. Lee, *Small*, 2023, **19**, 2206844.
27. K. Shah, R. Dai, M. Mateen, Z. Hassan, Z. Zhuang, C. Liu, M. Israr, W. C. Cheong, B. Hu and R. Tu, *Angew. Chem.*, 2022, **134**, e202114951.
28. Y. Hu, J. Zhou, X. Sun, J. Chen, B. Li, Y. Wang and N. Wang, *ChemCatChem*, 2022, **14**, e202201010.
29. G. Chen, T. Wang, J. Zhang, P. Liu, H. Sun, X. Zhuang, M. Chen and X. Feng, *Adv. Mater.*, 2018, **30**, 1706279.
30. Q. Yao, B. Huang, N. Zhang, M. Sun, Q. Shao and X. Huang, *Angew. Chem.*, 2019, **131**, 14121-14126.
31. Z. Zhuang, Y. Wang, C.-Q. Xu, S. Liu, C. Chen, Q. Peng, Z. Zhuang, H. Xiao, Y. Pan and S. Lu, *Nat. Commun.*, 2019, **10**, 4875.
32. Y. Wang, S. Wang, Z. L. Ma, L. T. Yan, X. B. Zhao, Y. Y. Xue, J. M. Huo, X. Yuan, S. N. Li and Q. G. Zhai, *Adva. Mater.*, 2022, **34**, 2107488.
33. J. Wang, L. Han, B. Huang, Q. Shao, H. L. Xin and X. Huang, *Nat. Commun.*, 2019, **10**, 5692.
34. L. Zhang, L. Wang, Y. Wen, F. Ni, B. Zhang and H. Peng, *Adv. Mater.*, 2020, **32**, 2002297.
35. H.-S. Park, J. Yang, M. K. Cho, Y. Lee, S. Cho, S.-D. Yim, B.-S. Kim, J. H. Jang and H.-K. Song, *Nano Energy*, 2019, **55**, 49-58.

36. M. Zhang, J. Chen, H. Li, P. Cai, Y. Li and Z. Wen, *Nano Energy*, 2019, **61**, 576-583.
37. S. Shin, T. U. Wi, T. H. Kong, C. Park, H. Lee, J. Jeong, E. Lee, S. Yoon, T. H. Kim and H. W. Lee, *Small*, 2023, **19**, 2206918.
38. C. Liu, B. Sheng, Q. Zhou, D. Cao, H. Ding, S. Chen, P. Zhang, Y. Xia, X. Wu and L. Song, *Nano Res.*, 2022, **15**, 7008-7015.
39. J. Xu, Z. Lian, B. Wei, Y. Li, O. Bondarchuk, N. Zhang, Z. Yu, A. Araujo, I. Amorim and Z. Wang, *ACS Catal.*, 2020, **10**, 3571-3579.
40. B. Jiang, X. Fan, Q. Dang, F. Liao, Y. Li, H. Lin, Z. Kang and M. Shao, *Nano Energy*, 2020, **76**, 105079.
41. K. Lu, G. Chang, H. Zhang and X.-Y. Yu, *Chem. Commun.*, 2021, **57**, 2907-2910.
42. N. Wang, S. Ning, X. Yu, D. Chen, Z. Li, J. Xu, H. Meng, D. Zhao, L. Li and Q. Liu, *Appl. Catal. B*, 2022, **302**, 120838.